Erciyes Üniversitesi
Fen Bilimleri Enstitüsü Dergisi
Cilt 41, Sayı 3, 2025

Erciyes University
Journal of Institue Of Science and Technology
Volume 41, Issue 3, 2025

Geant4 Simulation of Neutron Capture in Pure and Gadolinium-Doped Water for Neutrino Detectors

Mustafa Kandemir[*1]

[*1] Recep Tayyip Erdoğan Üniversitesi Fen Edebiyat Fakültesi Fizik, RİZE

(Alınış / Received: 07.10.2025, Kabul / Accepted: 24.11.2025, Online Yayınlanma / Published Online: 31.12.2025)

Keywords
Neutron capture time,
Netron capture radius,
Neutron track length,
Water Cherenkov detector,
Gd doping,
Geant4

Abstract: Neutron capture is a key process for detecting and characterizing neutrino interactions in large water-Cherenkov and gadolinium-doped detectors. Its timing and spatial signatures determine how efficiently delayed neutron signals can be separated from prompt backgrounds and therefore set fundamental limits on event reconstruction and background rejection. We present a detailed Geant4 (11.2.2) simulation of neutron capture in pure water and in water doped with 0.1 %, 0.2 %, and 0.5 % gadolinium (Gd) by mass. Primary neutrons were generated isotropically with three initial energy spectra—thermal (0.01–0.1 eV), intermediate (0.1 eV–100 keV), and fast (0.1–10 MeV)—each sampled with a uniform probability distribution. For every material–spectrum combination we recorded four observables: (i) mean neutron-capture time, (ii) capture-time distributions and their cumulative probabilities, (iii) total track length prior to capture, and (iv) capture radius relative to the primary neutron production vertex. The results show that at 0.5 % Gd, the mean capture time falls from roughly 200 μs in pure water to 5–9 μs across all neutron spectra, while the mean capture radius decreases from about 73 mm (thermal)–180 mm (fast) to 11 mm (thermal)–158 mm (fast). These findings quantify the dependence of capture dynamics on both absorber content and neutron energy and provide geometry-independent benchmarks—made possible by the use of a simulation volume large enough to ensure essentially complete neutron capture—for optimizing the time-window selection, fiducial-volume definition, and background suppression of next-generation neutrino detectors.

Nötrino Dedektörleri İçin Saf ve Gadolinyum Katkılı Suda Nötron Yakalanmasının Geant4 Simülasyonu

Anahtar Kelimeler
Nötron yakalanma süresi,
Nötron yakalanma yarıçapı,
Nötron iz uzunluğu,
Su Çerenkov dedektörü,
Gd katkılama,
Geant4

Öz: Nötron yakalanması, büyük su-Çerenkov ve gadolinyum katkılı dedektörlerde nötrino etkileşimlerini tespit etmek ve karakterize etmek için temel bir süreçtir. Bu olayın zamanlama ve konumsal imzaları, gecikmiş nötron sinyallerinin anlık arka planlardan ne kadar verimli ayrılabileceğini belirler ve bu nedenle olay yeniden yapılandırması ile arka plan bastırma üzerinde temel sınırlar koyar. Bu çalışmada, kütlece %0,1, %0,2 ve %0,5 gadolinyum (Gd) katkılı su ile saf sudaki nötron yakalanmasını ayrıntılı biçimde inceleyen bir Geant4 (11.2.2) simülasyonu sunulmaktadır. Birincil nötronlar, her biri üniform olasılık dağılımıyla örneklenen üç farklı başlangıç enerji spektrumunda—termal (0,01–0,1 eV), epitermal (0,1 eV–100 keV) ve hızlı (0,1–10 MeV)—izotropik olarak üretilmiştir. Her malzeme–spektrum kombinasyonu için dört gözlenebilir nicelik kaydedilmiştir: (i) ortalama nötron yakalanma süresi, (ii) yakalanma süresi dağılımları ve bunların kümülatif

olasılıkları, (iii) yakalanmadan önceki toplam iz uzunluğu ve (iv) nötronun oluştuğu noktaya göre yakalanma yarıçapı. Sonuçlar, %0,5 Gd derişiminde saf sudaki ortalama yakalanma süresinin yaklaşık 200 μs'ten tüm nötron spektrumları için 5–9 μs aralığına düştüğünü ve ortalama yakalanma yarıçapının ise yaklaşık 73 mm (termal)–180 mm (hızlı) değerlerinden 11 mm (termal)–158 mm (hızlı) aralığına gerilediğini göstermektedir. Bu bulgular, yakalanma dinamiklerinin hem soğurucu içeriğine hem de nötron enerjisine olan bağımlılığını nicelendirmektedir ve tüm nötronların neredeyse tamamen yakalanmasını sağlayacak kadar büyük bir simülasyon hacmi kullanılması sayesinde zaman aralığı seçiminin, faydalı hacim tanımının ve arka plan bastırmanın optimize edilmesi için geometriye bağımsız kıyas ölçütleri sunmaktadır.

1. Introduction

Large water-Cherenkov detectors are central to current and future neutrino physics programs, from long-baseline oscillation experiments to searches for supernova bursts and proton decay [1]. When a neutrino interacts in water it often produces free neutrons that diffuse and are captured on hydrogen or other nuclei, emitting delayed gamma rays. Measuring the time and spatial distribution of these captures is crucial for several reasons:

• Event tagging and background rejection. The delayed gamma signal following neutron capture provides a powerful handle to distinguish genuine neutrino interactions from uncorrelated radioactive or cosmogenic backgrounds. Accurate knowledge of the capture time spectrum determines the efficiency of such delayed-coincidence tags [2].

• Fiducial-volume definition and reconstruction. The distance a neutron travels before capture sets the minimum separation between the primary vertex and the delayed signal. This affects how close to detector boundaries an event can be reliably reconstructed and constrains systematic uncertainties in oscillation measurements [2].

• Optimization of gadolinium loading. Gadolinium has an exceptionally large thermal-neutron capture cross-section, reducing capture times by more than an order of magnitude and releasing a high-energy gamma cascade. Quantifying how capture time, track length, and capture radius depend on Gd concentration informs the trade-offs between cost, chemical stability, and physics performance in experiments such as Super-Kamiokande-Gd and future large-scale detectors [3-6].

Because these observables depend on both the incident neutron energy and the absorber content, their behavior must be understood before a detector is built. A detailed, geometry-independent simulation study provides exactly this insight: it allows the capture dynamics to be explored over a wide parameter space without the cost and complexity of hardware prototypes, and guides choices of fiducial volume, readout timing, and gadolinium concentration for future experiments.

This study also supports the ongoing reactor-neutrino research and detector-development efforts in Türkiye, particularly those associated with the Reactor Neutrino Experiments of Turkey (RNET) program [7, 8]. The RNET initiative encompasses the design and simulation of near-field detectors located close to the Akkuyu Nuclear Power Plant, including compact prototypes based on Water-based Liquid Scintillator (WbLS) technology. The simulation outcomes presented in this work provide valuable guidance for future improvements, especially regarding the incorporation of gadolinium into the detector medium and the optimization of detector performance for low-energy neutrino studies.

To model neutron capture in pure and gadolinium-doped water, we use the Geant4 toolkit (version 11.2.2). Primary neutrons are generated with initial energies from 0.01 eV to 10 MeV, spanning the full lifecycle of neutrino-produced neutrons—from their MeV-scale production energies down to the sub-eV thermal regime where capture occurs. This range also follows the classical neutron-energy classification of thermal (<0.1 eV), intermediate (0.1 eV–100 keV), and fast (>100 keV), ensuring that our results can be interpreted within established categories and encompass the energies most relevant to neutrino interactions and cosmic-ray spallation.

For each of these three representative regimes—thermal, intermediate, and fast—we generate large event samples and record four key observables: the mean capture time, the full capture-time distribution, the total track length, and the capture radius.

The following sections describe the simulation framework and physics models employed, present detailed comparisons of these observables across materials and energy spectra, and discuss how such simulation-driven benchmarks can inform the design and optimization of next-generation Gd-doped water-Cherenkov neutrino detectors.

2. Methodology

All simulations were carried out with the Geant4 toolkit [9,10] (version 11.2.2) to model neutron capture processes. For each combination of detector material (pure water or Gd-doped water at 0.1 %, 0.2 %, and 0.5 % by mass) and initial neutron spectrum (thermal, intermediate, and fast), 100 000 primary neutrons were generated to ensure statistically robust results. The objective was to extract geometry-independent neutron-capture observables—mean neutron capture time, full capture-time distributions, total track length, and capture radius—that can provide input for the design and optimization of large Gd-doped water-Cherenkov detectors.

2.1. Physics Models and Validation

High-precision (HP) neutron transport was used to model low-energy interactions. Before large-scale simulation production, several standard Geant4 physics lists—FTFP_BERT_HP, QGSP_BERT_HP, and QGSP_BIC_HP—were benchmarked to ensure consistent treatment of neutrons. The comparison showed that FTFP_BERT_HP and QGSP_BIC_HP produced nearly identical capture observables, whereas QGSP_BERT_HP yielded markedly different capture times and spatial distributions.

Subsequent investigation revealed that the discrepancy originated from a known issue in the HP neutron treatment of the QGSP_BERT_HP physics list in Geant4 11.2.2. This problem, reported by a user and documented on the Geant4 official forum, led us to adopt FTFP_BERT_HP for all production simulations to ensure reliable and consistent results.

2.2. Geometry setup

A simple, large-volume detector geometry (with both diameter and height chosen sufficiently large, $>10^6$ mm) was implemented so that nearly all primary neutrons were captured before escaping the simulation world, This choice allows the extracted capture characteristics to be interpreted as geometry-independent bulk material properties. Four material configurations were studied: (1) pure water (H_2O) and (2–4) gadolinium-doped water with gadolinium concentrations of 0.1 %, 0.2 %, and 0.5 % by mass. The gadolinium doping fraction was chosen in line with values typically considered in large-scale neutrino experiments [11-14]. The inclusion of gadolinium, with its exceptionally large thermal-neutron capture cross section, is of particular interest for next-generation neutrino detectors.

2.3. Neutron source

Neutrons were generated with the General Particle Source (GPS) module in Geant4. The source was placed at the center of the water volume, and neutrons were emitted isotropically. To represent the main regimes relevant to neutron studies in neutrino detectors, three energy intervals were defined: thermal (0.01–0.1 eV), intermediate (0.1 eV–100 keV), and fast (0.1 MeV–10 MeV). For each spectrum, a linear energy distribution with uniform probability was used across the specified range.

2.3. Observables

For every combination of neutron spectrum and detector medium, four key observables were recorded for neutrons that underwent capture:

• Mean neutron capture time: A binned mean profile was constructed to obtain the average capture time for each initial-energy bin, providing the mean capture time as a function of the neutron's initial energy.

• Neutron capture time : A normalized histogram of individual capture times was produced, accompanied by a cumulative-probability histogram showing, for any capture-time threshold, the probability that a single neutron is captured within that time.

• Neutron track length: The total path length travelled by a neutron before capture, derived from step-by-step tracking.

• Neutron capture radius: The straight-line displacement between the neutron's creation point and its capture location,

For observables (2) and (4), both the standard histograms and their corresponding cumulative distributions were produced, in order to better capture the probability of neutron capture within a given time window and radial distance.

Track length and capture radius were analyzed separately to distinguish the actual path travelled from the net spatial displacement, parameters that are critical for defining fiducial volumes and evaluating detection efficiency in large water-Cherenkov or Gd-doped neutrino detectors.

3. Results

3.1. Mean neutron capture time

Figures 1–3 show the mean neutron-capture time as a function of the initial neutron energy for thermal, intermediate, and fast neutron spectra, in pure water and in water doped with gadolinium at concentrations of 0.1 %, 0.2 %, and 0.5 % by mass, respectively. Each figure is binned in initial-energy intervals; the horizontal extent of a point represents the width of the corresponding energy bin, while the vertical coordinate shows the average capture time of neutrons whose initial energies fall within that bin.

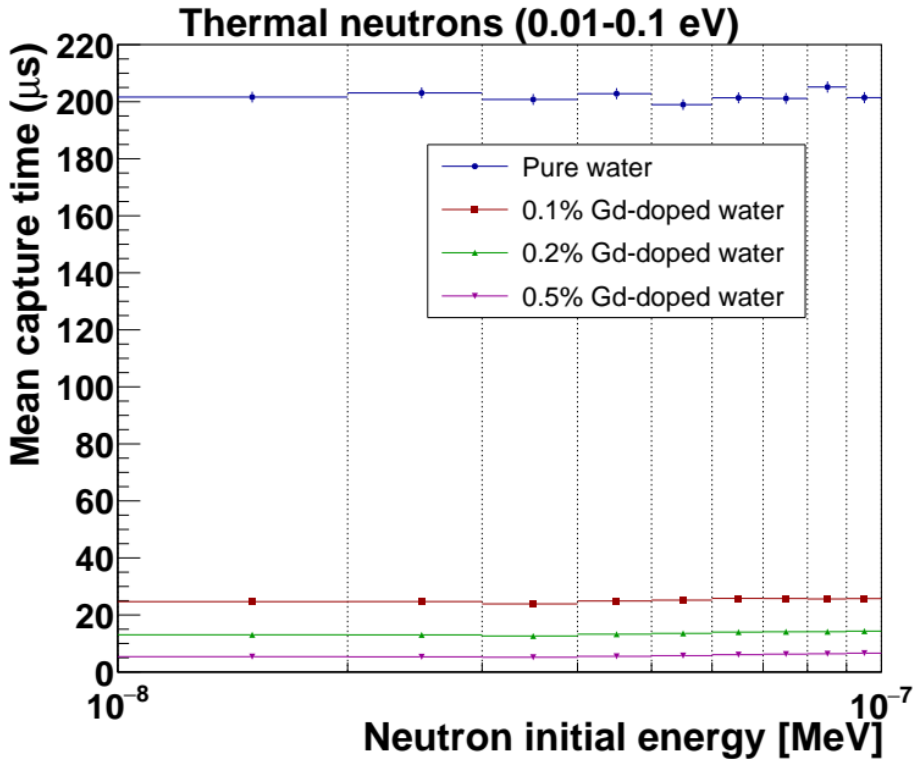

Figure 1. Mean neutron-capture time as a function of initial neutron energy for thermal neutrons (0.01–0.1 eV) in pure water and in gadolinium-doped water with 0.1 %, 0.2 %, and 0.5 % Gd by mass. Data points represent averages within logarithmic energy bins; horizontal bars show the bin width and vertical coordinates give the mean capture time of neutrons born in that bin.

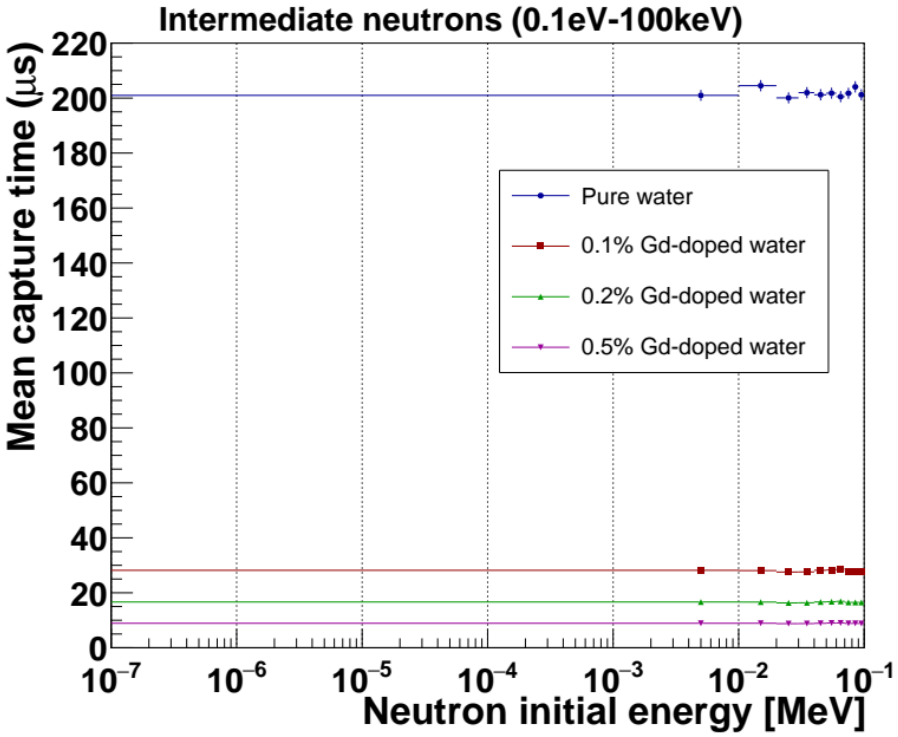

Figure 2. Mean neutron-capture time as a function of initial neutron energy for intermediate neutrons (0.1 eV–100 keV) in pure water and in gadolinium-doped water with 0.1 %, 0.2 %, and 0.5 % Gd by mass. Data points represent averages within logarithmic energy bins; horizontal bars show the bin width and vertical coordinates give the mean capture time of neutrons born in that bin.

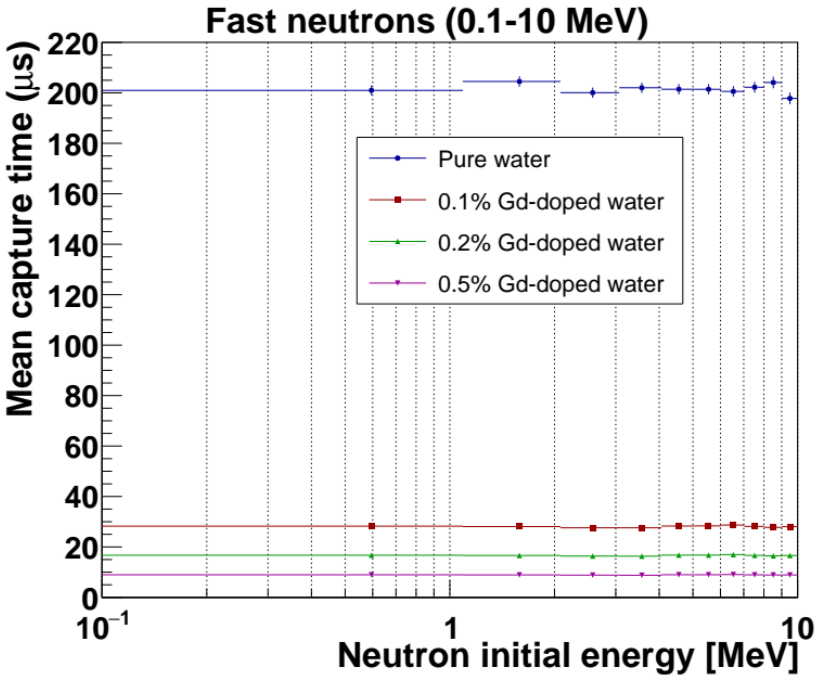

Figure 3. Mean neutron-capture time as a function of initial neutron energy for fast neutrons (0.1–10 MeV) in pure water and in gadolinium-doped water with 0.1 %, 0.2 %, and 0.5 % Gd by mass. Data points represent averages within logarithmic energy bins; horizontal bars show the bin width and vertical coordinates give the mean capture time of neutrons born in that bin.

In pure water the three curves are virtually identical across all figures confirming that the capture time is set by the material properties and shows no significiant dependence on the neutron's initial energy.

For gadolinium-doped water the trends are broadly similar across energies: the 0.1 %, 0.2 %, and 0.5 % curves nearly overlap from fast to intermediate energies, with only a slight additional reduction for thermal neutrons. Adding gadolinium to pure water at a concentration of 0.1 % lowers the mean neutron-capture time from roughly 200 μs in pure water to about 20–30 μs across all three neutron spectra, while raising the concentration from 0.1 % to 0.5 % further shortens the mean capture time to roughly 5–9 μs, depending on the spectrum. The weak dependence on the initial neutron energy suggests that these results may be applicable to neutrons of different origins in large water-Cherenkov detectors.

3.2. Neutron capture time distribution

Figures 4–6 present the full neutron-capture time distributions for thermal, intermediate, and fast initial spectra, each paired with its cumulative-probability curve. Unlike the binned mean profiles of Section 3.1, these plots show the entire event–by–event capture-time spectrum. The left panel in each figure gives the normalized capture-time histogram, while the right panel displays the corresponding cumulative probability: the horizontal coordinate is the capture time and the vertical value gives the probability that a single neutron is captured within that time window. Mean values for each medium—reported directly on the plots—match those inferred from the mean-capture-time analysis of Figures 1–3.

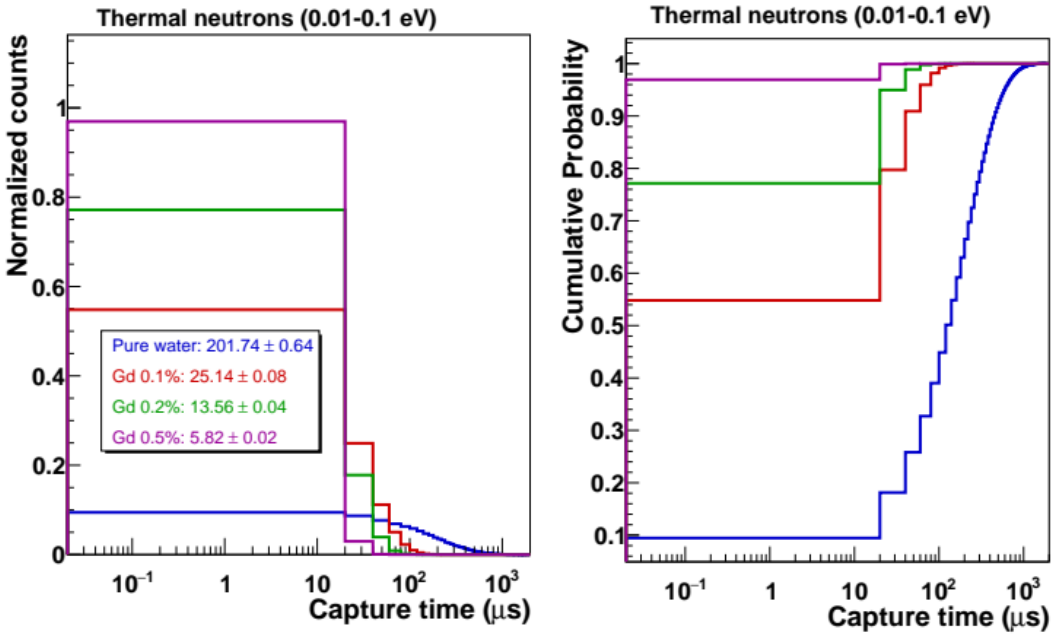

Figure 4. Normalized neutron-capture time distribution (left) and cumulative probability (right) for thermal neutrons (0.01–0.1 eV) in pure water and Gd-doped water (0.1 %, 0.2 %, 0.5 % by mass).

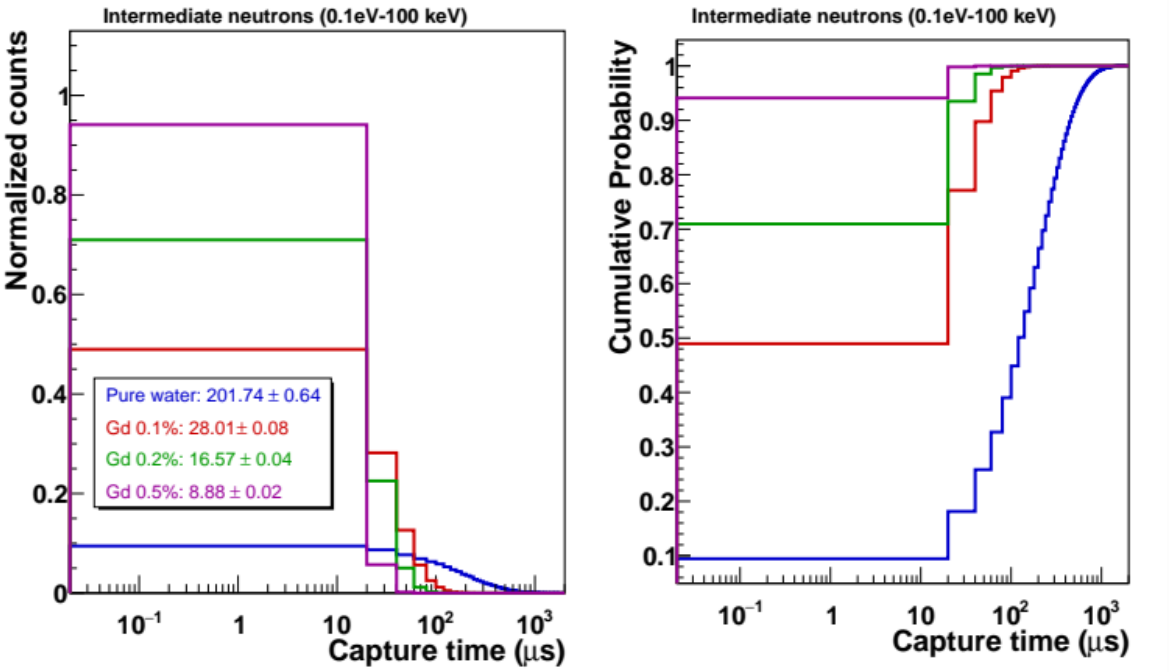

Figure 5. Normalized neutron-capture time distribution (left) and cumulative probability (right) for intermediate neutrons (0.1 eV–100 keV) in pure water and Gd-doped water (0.1 %, 0.2 %, 0.5 % by mass).

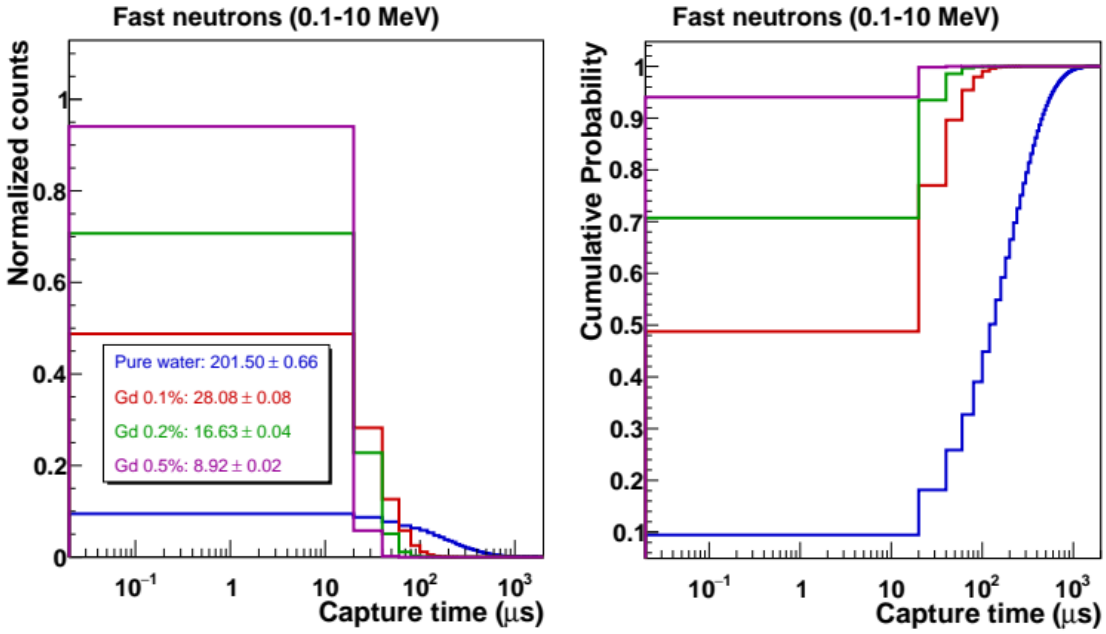

Figure 6. Normalized neutron-capture time distribution (left) and cumulative probability (right) for fast neutrons (0.1–10 MeV) in pure water and Gd-doped water (0.1 %, 0.2 %, 0.5 % by mass).

The cumulative curves provide a direct measure of the likelihood that a neutron is captured within specific time intervals, information that is critical for defining delayed-coincidence trigger windows in large detectors. Table 1 summarizes these probabilities for capture within 40, 80, 120, and 160 μs across all energy spectra and materials. For pure water, only about 18 % of neutrons capture within 40 μs, rising to roughly 55 % by 160 μs, whereas adding just 0.1 % Gd increases the 40 μs capture probability to nearly 80 % and the 160 μs probability to ≳99 %. Higher Gd concentrations push these probabilities effectively to 100 % across all spectra. These results emphasize

that, while the overall shapes of the capture-time distributions remain similar for thermal, intermediate, and fast neutrons, gadolinium loading—rather than the initial neutron energy—governs the timing characteristics relevant for detector design and background rejection.

Table 1. Cumulative probability of neutron capture within selected time windows (≤ 40 μs, ≤ 80 μs, ≤ 120 μs, and ≤ 160 μs) for thermal, intermediate, and fast neutron spectra in pure water and in gadolinium-doped water with 0.1 %, 0.2 %, and 0.5 % Gd by mass. Probabilities are derived from the cumulative capture-time distributions shown in Figures 4–6.

Spectrum	Medium	≤ 40 μs	≤ 80 μs	≤ 120 μs	≤ 160 μs
Thermal	Pure Water	18.1	32.7	44.9	54.9
	Gd 0.1%	79.7	95.9	99.2	99.8
	Gd 0.2%	95.0	99.7	100.0	100.0
	Gd 0.5%	99.9	100.0	100.0	100.0
Intermediate	Pure Water	18.1	32.7	44.9	54.9
	Gd 0.1%	77.1	95.4	99.1	99.8
	Gd 0.2%	93.5	99.7	100.0	100.0
	Gd 0.5%	99.8	100.0	100.0	100.0
Fast	Pure Water	18.1	32.7	44.9	54.9
	Gd 0.1%	77.0	95.4	99.1	99.8
	Gd 0.2%	93.5	99.7	100.0	100.0
	Gd 0.5%	99.8	100.0	100.0	100.0

3.3. Neutron track length

Figures 7–9 display the distributions of total neutron track length, defined as the complete path a neutron travels before capture, for thermal, intermediate, and fast initial spectra. Each figure presents a normalized track-length histogram together with its cumulative-probability curve, arranged side by side as in the capture-time plots of Section 3.2. The horizontal axis gives the total distance traversed before capture, while the right-hand cumulative panel shows the probability that a single neutron is captured within a path length shorter than the indicated value. Mean track-length values for each medium are reported directly on the plots.

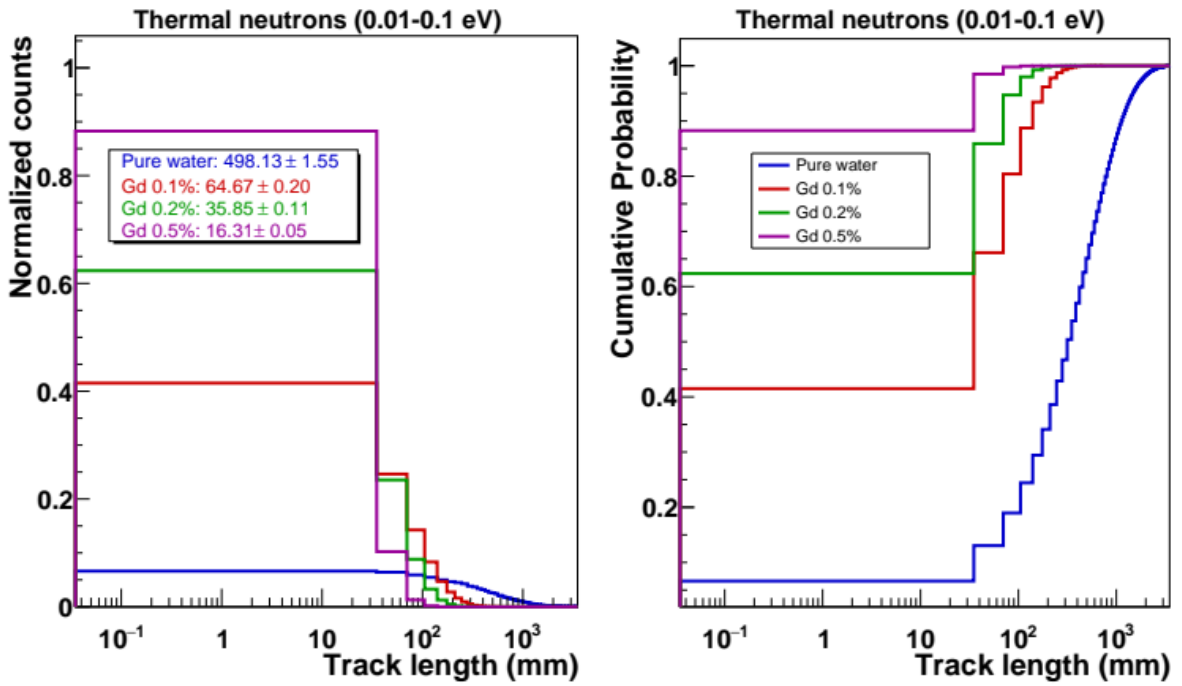

Figure 7: Total neutron track-length distribution and cumulative probability for thermal neutrons (0.01–0.1 eV) in pure water and Gd-doped water (0.1 %, 0.2 %, 0.5 % by mass).

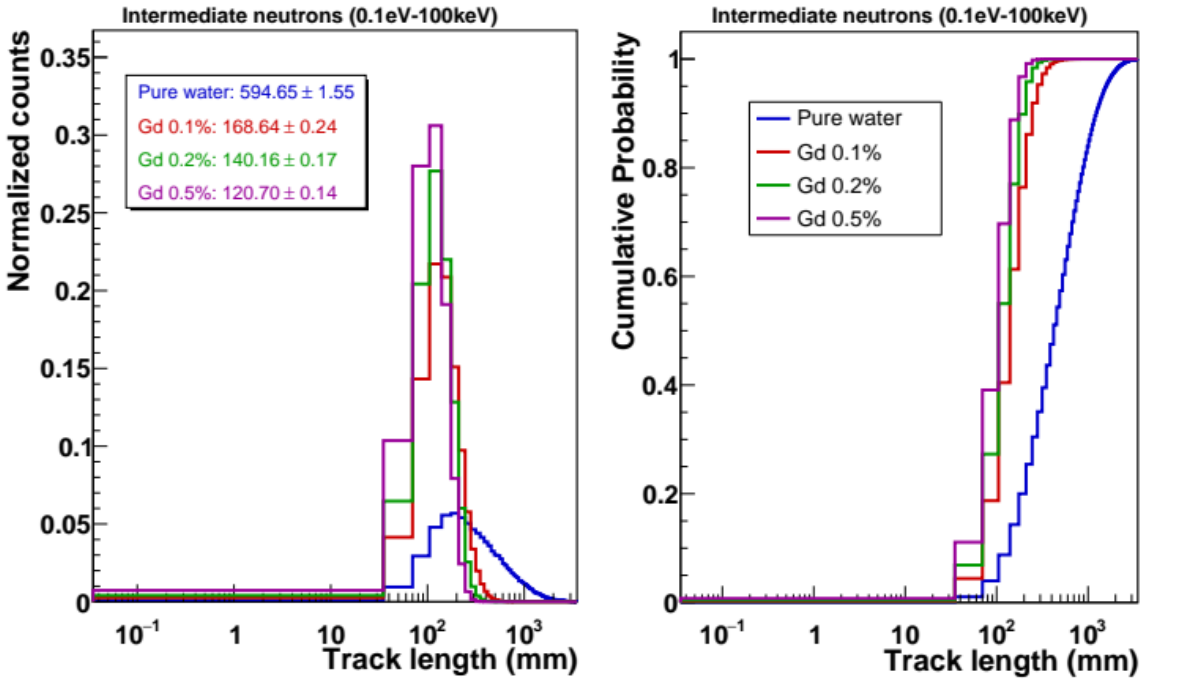

Figure 8. Total neutron track-length distribution and cumulative probability for intermediate neutrons (0.1 eV–100 keV) in pure water and Gd-doped water (0.1 %, 0.2 %, 0.5 % by mass).

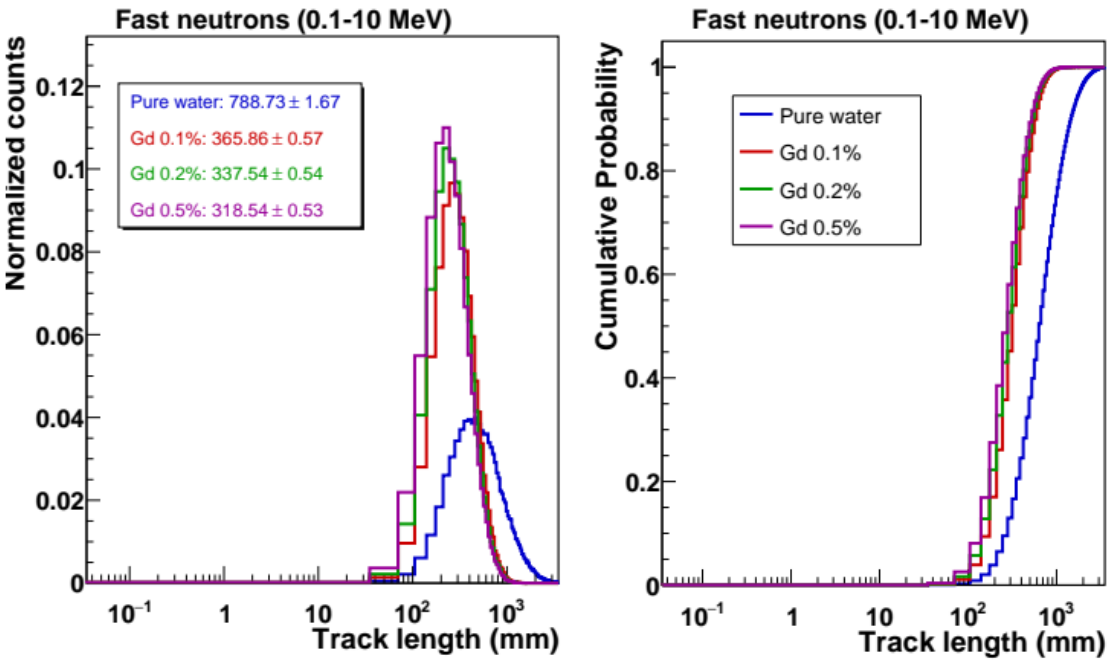

Figure 9. Total neutron track-length distribution and cumulative probability for fast neutrons (0.1–10 MeV) in pure water and Gd-doped water (0.1 %, 0.2 %, 0.5 % by mass).

In contrast to the capture-time results, which showed only minimal dependence on the initial neutron spectrum, the total distance travelled before capture varies strongly with the starting energy. In pure water the mean track length increases from roughly 500 mm for thermal neutrons to about 600 mm for intermediate neutrons and nearly 790 mm for fast neutrons, reflecting the longer moderation paths required for higher-energy neutrons. Adding gadolinium shortens these paths dramatically—down to about 65 mm (0.1 % Gd), 36 mm (0.2 % Gd), and 16 mm (0.5 % Gd) for thermal neutrons, with corresponding mean lengths of roughly 170 mm, 140 mm, and 120 mm for intermediate neutrons, and 370 mm, 340 mm, and 320 mm for fast neutrons. The persistent ordering—fast > intermediate > thermal—demonstrates that although all neutrons ultimately thermalize before capture, those created at higher energies must traverse longer paths while slowing down.

These observations underscore a subtle but important point: the small microsecond-level differences in capture time observed across neutron spectra (Section 3.2) translate into tens of centimeters of additional travel distance. Thus, even when capture times appear nearly identical, neutrons of higher initial energy can travel significantly farther through the detector. This distinction highlights the need to consider both temporal and spatial observables when defining fiducial volumes and assessing edge effects in large water-Cherenkov detectors, where the separation between the primary interaction point and the delayed capture signal constrains event reconstruction and background rejection.

3.4. Neutron capture radius

Figures 10–12 present the distributions of neutron capture radius, defined as the straight-line displacement between a neutron's creation point and its capture location, for thermal, intermediate, and fast initial spectra. As in the capture-time and track-length analyses, each figure combines a normalized capture-radius histogram with its cumulative-probability curve, enabling both differential and integral views of the data. The horizontal axis gives the radial distance from the source to the capture point, while the cumulative panel shows the probability that a single neutron is captured within a radius smaller than the indicated value. Mean capture-radius values for each medium are reported directly on the plots: about 73 mm for thermal, 94 mm for intermediate, and 179 mm for fast neutrons in pure water, decreasing with gadolinium loading to roughly 25 mm, 18 mm, and 11 mm (thermal), 60 mm, 57 mm, and 55 mm (intermediate), and 160 mm, 159 mm, and 158 mm (fast) for 0.1 %, 0.2 %, and 0.5 % Gd, respectively.

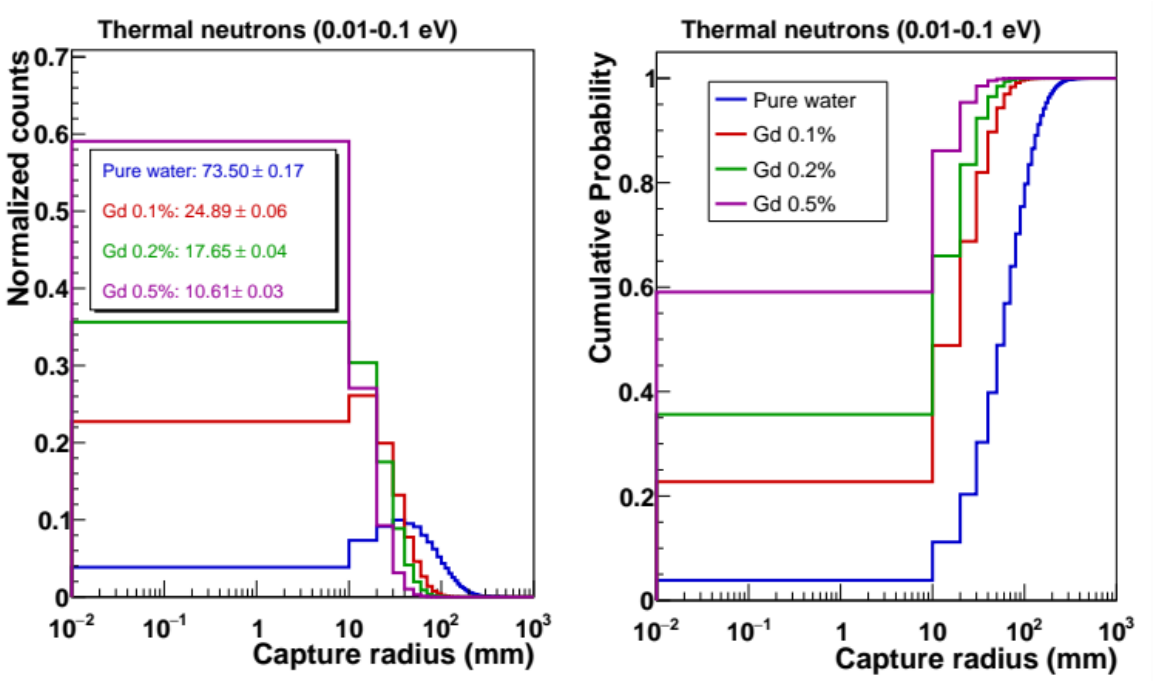

Figure 10. Neutron capture-radius distribution and cumulative probability for thermal neutrons (0.01–0.1 eV) in pure water and in gadolinium-doped water (0.1 %, 0.2 %, 0.5 % by mass).

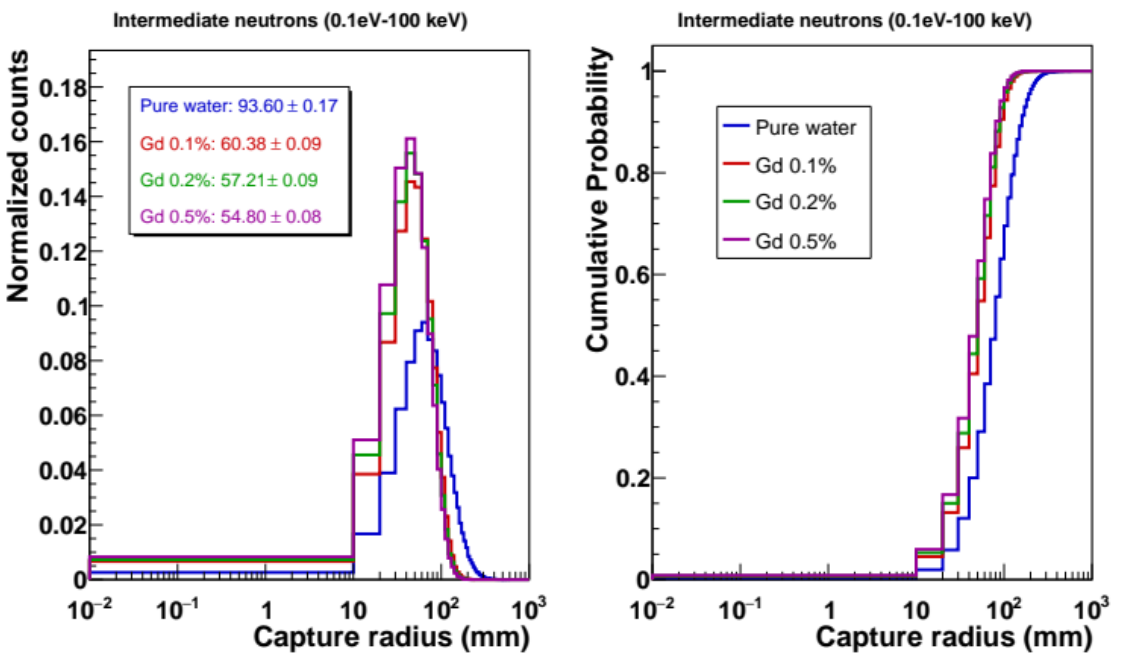

Figure 11. Neutron capture-radius distribution and cumulative probability for intermediate neutrons (0.1 eV–100 keV) in pure water and in gadolinium-doped water (0.1 %, 0.2 %, 0.5 % by mass).

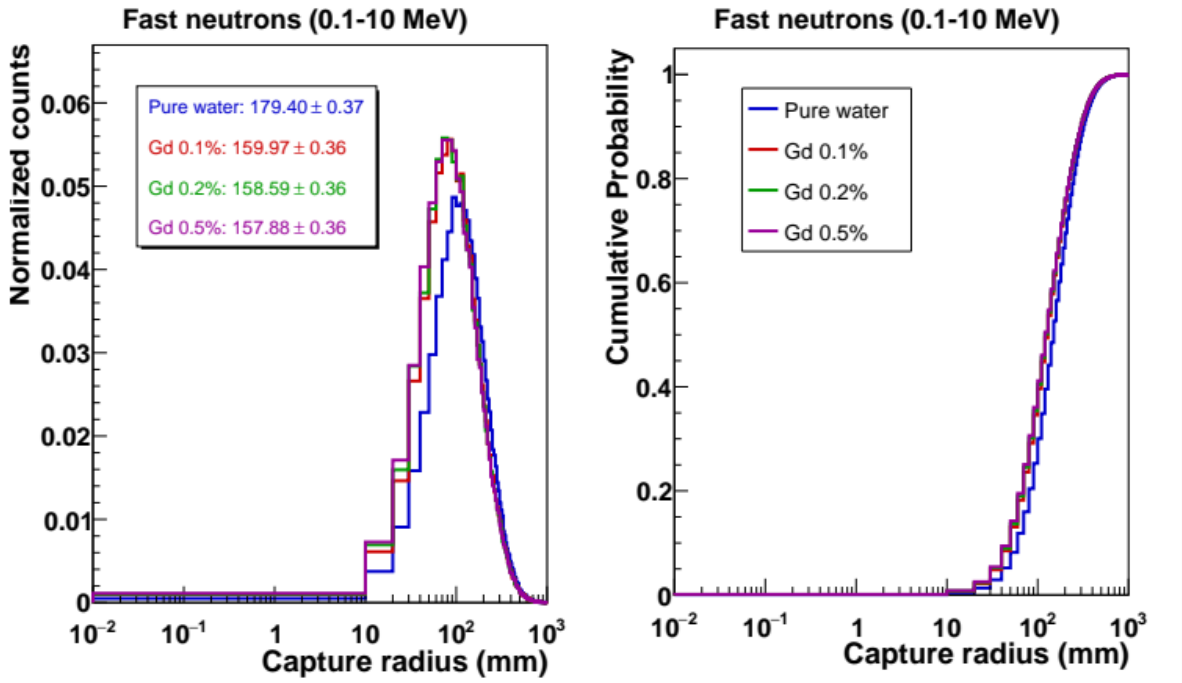

Figure 12. Neutron capture-radius distribution and cumulative probability for fast neutrons (0.1–10 MeV) in pure water and in gadolinium-doped water (0.1 %, 0.2 %, 0.5 % by mass).

These results highlight the distinction between track length (Section 3.3) and capture radius. Track length measures the total path a neutron travels before capture, whereas capture radius quantifies only the net spatial displacement. A neutron may follow a long trajectory yet still be captured close to its generation vertex, so the capture radius is always smaller than the track length. The dependence on initial energy is nonetheless clear: higher-energy neutrons exhibit broader capture-radius distributions even though their capture times remain almost identical on the microsecond scale.

Table 2 summarizes the cumulative probabilities of capture within 20, 40, 60, and 80 mm for all spectra and gadolinium concentrations, derived from the cumulative curves of Figures 10–12. For thermal neutrons in pure water, only 11 % capture within 20 mm and 64 % within 80 mm, while adding just 0.1 % Gd raises these probabilities to 49 % and 98 %, respectively. At 0.5 % Gd the 20 mm probability reaches 86 % and the 80 mm probability essentially 100 %. Intermediate neutrons show lower confinement, with pure water yielding 1.9 % within 20 mm and 47 % within 80 mm, improving to 5.9 % and 84 % at 0.5 % Gd. Fast neutrons remain the most diffuse, with pure water giving only 0.4 % within 20 mm and 16 % within 80 mm; even at 0.5 % Gd these values rise only to 0.8 % and 25 %, respectively.

These findings confirm that capture radius—not track length—is the key metric for defining fiducial volumes in large water-Cherenkov detectors. While gadolinium concentration governs the overall scale of the displacement, the initial neutron energy determines how far the capture point can drift from the primary interaction vertex. Accurate knowledge of this spatial separation is essential for setting detector margins, mitigating edge effects, and ensuring robust event reconstruction.

Table 2. Cumulative probability of neutron capture within specified radial distances (in mm) for different initial energy spectra and gadolinium concentrations.

Spectrum	Medium	≤ 20 mm	≤ 40 mm	≤ 60 mm	≤ 80 mm
Thermal	Pure water	11.2	30.3	48.9	64.0
	Gd 0.1 %	48.8	82.0	94.3	98.4
	Gd 0.2 %	66.0	92.4	98.5	99.7
	Gd 0.5 %	86.1	98.5	99.8	100.0
Intermediate	Pure water	1.9	12.1	29.1	47.3
	Gd 0.1 %	4.5	25.9	54.8	77.4
	Gd 0.2 %	5.3	28.8	59.2	81.1
	Gd 0.5 %	5.9	31.8	62.7	83.8
Fast	Pure water	0.4	2.9	8.2	16.0
	Gd 0.1 %	0.7	4.8	13.1	23.6
	Gd 0.2 %	0.8	5.2	13.7	24.6
	Gd 0.5 %	0.8	5.4	14.2	25.1

4. Discussion and Conclusion

We have performed a detailed Geant4 (version 11.2.2) study of neutron capture in pure water and in water doped with 0.1 %, 0.2 %, and 0.5 % gadolinium by mass, using three representative initial neutron spectra: thermal (0.01–0.1 eV), intermediate (0.1 eV–100 keV), and fast (0.1–10 MeV). The simulations quantify how gadolinium concentration and incident neutron energy affect capture time, cumulative capture probability, total track length, and radial capture distance.

The simulations also demonstrate that the capture radius—the net displacement between the neutron's creation and capture points—is highly sensitive to both gadolinium concentration and the neutron's starting energy. While gadolinium markedly contracts the overall scale of this displacement, higher-energy neutrons retain broader capture-radius distributions, underscoring the need to consider initial energy when defining fiducial volumes.

These geometry-independent benchmarks confirm that gadolinium concentration controls the timing of delayed signals, while the capture radius defines the key spatial distance between the primary interaction point and the delayed gamma emission. Taken together, these results give practical guidance for setting delayed-coincidence time windows and defining fiducial volumes in next-generation water-Cherenkov neutrino detectors.

References

[1] Fukuda, S., et al. 2003. The Super-Kamiokande detector. Nuclear Instruments and Methods in Physics Research Section A: Accelerators, Spectrometers, Detectors and Associated Equipment, 501 (2), 418–462

[2] Abe, K., et al. 2022. Neutron tagging following atmospheric neutrino events in a water Cherenkov detector. Journal of Instrumentation, 17 (10), P10029.

[3] Beacom, J. F., & Vagins, M. R. 2004. Antineutrino spectroscopy with large water Čerenkov detectors. Physical Review Letters, 93 (17), 171101.

[4] Abe, K., et al. 2022. First gadolinium loading to Super-Kamiokande. Nuclear Instruments and Methods in Physics Research Section A: Accelerators, Spectrometers, Detectors and Associated Equipment, 1027, 166248.

[5] Marti, Ll., et al. 2020. Evaluation of gadolinium's action on water Cherenkov detector systems with EGADS. Nuclear Instruments and Methods in Physics Research Section A: Accelerators, Spectrometers, Detectors and Associated Equipment, 959, 163549.

[6] Abe, K., et al. 2024. Second gadolinium loading to Super-Kamiokande. Nuclear Instruments and Methods in Physics Research Section A: Accelerators, Spectrometers, Detectors and Associated Equipment, 1065, 169480.

[7] Bat, A., Tiras, E., Fischer, V. *et al.* Low energy neutrino detection with a compact water-based liquid scintillator detector. *Eur. Phys. J. C* **82**, 734 (2022).

[8] Fischer, V., & Tiras, E. 2020. Water-based Liquid Scintillator detector as a new technology testbed for neutrino studies in Turkey. *Nuclear Instruments and Methods in Physics Research Section A: Accelerators, Spectrometers, Detectors and Associated Equipment*, **969**, 163931.

[9] Allison, J., Amako, K., Apostolakis, J., et al. 2016. Recent developments in Geant4. Nuclear Instruments and Methods in Physics Research Section A: Accelerators, Spectrometers, Detectors and Associated Equipment, 835, 186–225.

[10] Allison, J., Amako, K., Apostolakis, J., et al. 2006. Geant4 developments and applications. IEEE Transactions on Nuclear Science, 53 (1), 270–278

[11] Lasorak, P., & Prouse, N. 2015. TITUS: An Intermediate Distance Detector for the Hyper-Kamiokande Neutrino Beam. ArXiv:1504.08272.

[12] Marti, Ll., et al. 2020. Evaluation of gadolinium's action on water Cherenkov detector systems with EGADS. Nuclear Instruments and Methods in Physics Research Section A: Accelerators, Spectrometers, Detectors and Associated Equipment, 959, 163549

[13] Li, V. A., Dazeley, S. A., Bergevin, M., & Bernstein, A. 2022. Scalability of gadolinium-doped-water Cherenkov detectors for nuclear nonproliferation. Physical Review Applied, 18 (3), 034059.

[14] Back, A. R., et al. 2017. Accelerator Neutrino Neutron Interaction Experiment (ANNIE): Preliminary Results and Physics Phase Proposal. arXiv:1707.08222.